

A Ranking Method for Neutral Pion Selection in
High Multiplicity Hadronic Events

Ph. D thesis work, second report.

Ahmet BİNGÜL

3rd January 2002

Supervisor:

Assist. Prof. Dr. Ayda BEDDALL

Department of Engineering Physics
University of Gaziantep

Abstract

A Ranking Method for Neutral Pion Selection in High Multiplicity Hadronic Events

BİNGÜL, Ahmet

Ph. D thesis work, second report.

Supervisor: Assist. Prof. Dr. Ayda BEDDALL

3rd January 2002

The selection of neutral pions with a high purity while maintaining also a high efficiency can be important in the formation of statistically significant mass spectra in the reconstruction of short-lived particles such as the omega meson ($\omega \rightarrow \pi^+\pi^-\pi^0$). In this study a Ranking method is described and detailed results from a Monte-Carlo study are presented. The results show that the Ranking method, when applied to high multiplicity events, yields significant improvements in the purity of selected pion candidates and facilitates the relaxation of standard cuts thereby avoiding some systematic uncertainties.

Table of Contents

Chapter

1	Introduction	1
2	Particle Physics and Particle Detectors	4
2.1	Introduction	4
2.2	The ALEPH Detector	4
2.2.1	Overview	5
2.2.2	The Central Tracking Chambers	5
2.2.3	The Principal Calorimeters	7
3	Pion Reconstruction and Initial Selection	9
3.1	Mass Constraint	11
4	A Pion Estimator	13
4.1	Estimator Application Methods	15
	References	16
	Appendix	
A	Directory Tree-Structure	17
	Publications	18

List of Tables

Table

- | | | |
|-----|---|----|
| 2.1 | Tracking momentum and impact parameter resolution. | 7 |
| 4.1 | Comparison of purity and efficiency. The stochastic term, R , in the detector resolution, and the event energy, are varied. | 15 |

List of Figures

Figure

1.1	Reconstruction of a typical hadronic event in the ALEPH detector	2
2.1	Helix parameters used in the TPC tracking algorithms	6
3.1	Invariant mass of photon pairs at CM energy of 91.2 <i>GeV</i>	10
4.1	Chi-square versus photon pair opening angle (for each candidate)	14
A.1	A typical user's directory tree (not complete)	17

List of Symbols

e^- : Electron

e^+ : Positron

ω : Omega Vector Meson

π^+ : Positively charged pi-meson

π^- : Negatively charged pi-meson

π^0 : Neutral pi-meson

γ : Photon

θ_{12} : Opening angle of the photons

E : Electromagnetic shower energy (in *GeV*)

σ : Gaussian width

σ : Cross-section

σ_N : Energy equivalent of electronic noise

σ_M : Gaussian mass width of the pion signal

σ_1 : Error on first photon

σ_2 : Error on second photon

$\sigma_{\theta,\phi}$: Angular resolution

$\sigma_{r,\phi}$: Spatial resolution

σ_E : Energy resolution

ΔE : Energy resolution

and so on...

Chapter 1

Introduction

What follows is an extract from a thesis latexed with the `G.U. thesis.cls` class file; it is given here as an example for latexing with the `phd-report.cls` class file and is not intended to be an example of a PhD report.

High energy collisions of sub-atomic particles can result in events containing a high multiplicity of hadronic particles. An example of such an event is the production of Z Bosons at LEP, an e^+e^- collider with a center of mass (CM) energy of 91.2 GeV , where the subsequent hadronic decay of the Z Boson results in two or more jets of particles with a total event multiplicity of, on average, about 30 particles mostly charged and neutral pions, Figure 1.1.

Invariant mass spectra, constructed from selected particle tracks, reveal the presence of short-lived ‘mother’ particles which present themselves as peaks on a combinatorial background. One example is the decay of the omega vector meson (mass $782\text{ MeV}/c^2$) to three pions: $\omega \rightarrow \pi^+\pi^-\pi^0$. The ω is reconstructed from measurements of the momentum of the daughter particles; charged pions are measured in a tracking chamber with good momentum resolution while the neutral pion, decaying mainly via the two-photon channel $\pi^0 \rightarrow \gamma\gamma$, is reconstructed from measurements of its daughter photons in a calorimeter typically with much poorer momentum resolution. Measurements of the ω and other examples can be found in [1].

The selection of neutral pions with a high purity while maintaining also a high efficiency can be important in the formation of statistically significant mass spectra. Neutral pion reconstruction plays a dominant role in the resultant purity and momentum resolution of reconstructed mother particles. Pion momentum resolution tends to be poor due to calorimeter resolution, purity tends to be low due to a large combinatorial background from wrong combinations of photon pairs, a situation which becomes worse for higher multiplicity events and poorer calorimeter resolution. This thesis presents a study of a Ranking method for significantly increasing the purity of reconstructed neutral pions. This is achieved

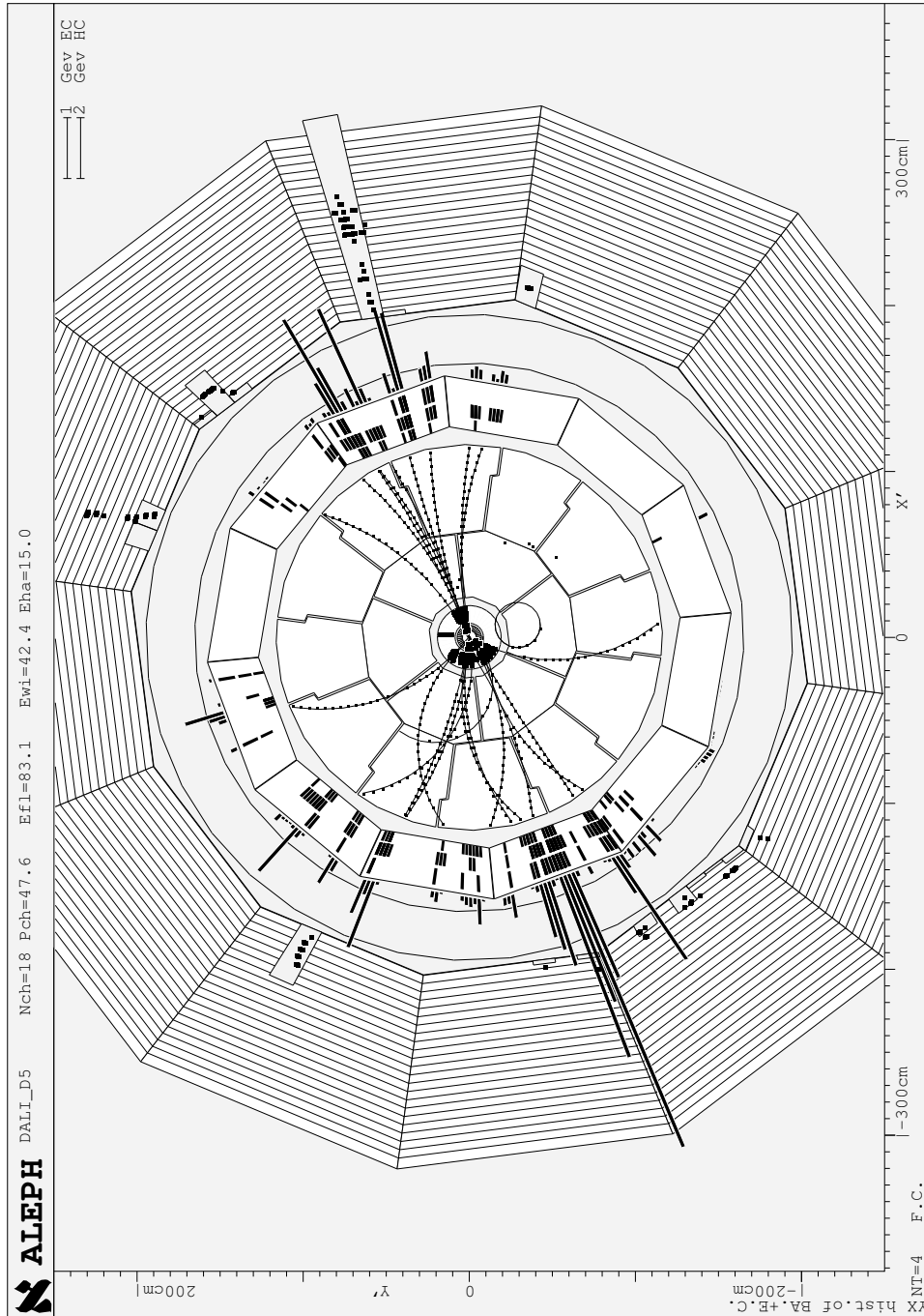


Figure 1.1: Reconstruction of a typical hadronic event in ALEPH detector. The distinguishing feature of hadronic events is large multiplicity of visible particles and a large fraction of the center of mass energy that they carry. The overall reconstructed energy in this event is 83 GeV , the charged component totals 48 GeV from 18 tracks.

by identifying and removing background formed by incorrect combinations of photon pairs.

First, an overview of particle physics and particle detectors is given in Chapter 2; some emphasis is placed on the ALEPH detector as monte-carlo simulations used in this thesis are based on this experiment. *And so on...*

Chapter 2

Particle Physics and Particle Detectors

2.1 Introduction

The modern physicist working in elementary particle research is continuing a quest for understanding of the basic structure of matter which has gone on for thousands of years. *And so on*

2.2 The ALEPH Detector

ALEPH (Apparatus for LEP pHysics) was one of four detectors positioned around the LEP collider at CERN. It was in operation for six years in the study of e^+e^- collisions at Z resonance. The ALEPH project was the outcome of a collaboration of several hundred physicists and engineers from thirty universities and national laboratories, principally from Europe but also from China and the U.S.A. Detailed performance of the ALEPH detector can be found in [5] and [6].

ALEPH is a particle detector, covering as much of the 4π solid angle as possible. It is designed to measure the momenta of charged particles, to measure the energy deposited in calorimeters by charged and neutral particles, to identify the three lepton flavors, and to measure the distance of travel of short-lived particles such as the tau lepton and the b and c hadrons. Particular emphasis has been given to momentum resolution up to the highest energies (by means of a large tracking system in a 1.7 T magnetic field), to electron identification (by means of a high segmented, projective electromagnetic calorimeter, as well as ionization measurement in the tracing system), and muon identification (with continuous tracing inside sufficient iron absorber to eliminate the hadrons).

2.2.1 Overview

ALEPH uses a coordinate system usually expressed in terms of Cartesian (x, y, z) or cylindrical (r, ϕ, z) coordinates. In both cases, the z direction is along the beam line with the e^- direction defining the positive axis. The positive x direction points to the centre of LEP and the positive y direction is defined such that (x, y, z) forms a right-handed coordinate system.

The tracking system involves three subdetectors: a silicon vertex detector, a drift chamber with 30 *cm* outer radius, which is also important as part of the trigger system, and a time projection chamber with 180 *cm* outer radius. Calorimetry proceeds in two stages: electromagnetic and hadronic. A muon detection system of two double-layers of streamer tubes surrounds the whole detector. Finally, important for precise cross-section measurement are the highly segmented luminosity calorimeters.

Presented here is a summary of the main features of the apparatus, more detailed accounts can be found elsewhere [6], [7].

2.2.2 The Central Tracking Chambers

The Vertex Detector (VDET)

Close to the interaction point, tracking is performed by a silicon vertex detector. Vertex detector hits are used to provide additional precision for tracks already reconstructed in the outer tracking.

The device is formed from 96 silicon wafers each of dimensions $(5.12 \times 5.12 \times 0.03)$ *cm*, arranged in two coaxial cylinders around the beam pipe. The spatial resolution, for normally incident tracks is: $\sigma_{r\phi} \approx 12 \mu m$, $\sigma_z \approx 10 \mu m$.

The Inner Tracking Chamber (ITC)

The vertex detector is surrounded by a conventional cylindrical multiwire drift chamber. It measures the $r\phi$ position of a track on eight concentric layers of hexagonal drift cells at radii between 16 and 26 *cm*, with adjacent layers staggered by half a cell width. The resolution depends on the drift length in the cell, with an average of 150 μm . The position of tracks along the beam direction (z) is determined by measuring the difference in arrival time of the signals at each end of the wires. This, however, only has a resolution of a few centimetres. The ITC tracking information is used to improve tracking resolution, and to provide information for the first level trigger decision (made within 2-3 μs after a beam crossing).

The Time Projection Chamber (TPC)

The TPC is ALEPH's principal tracking detector providing 21 3D space-point measurements for fully contained tracks at radii between 30 and 180 *cm*. It consists of a gas volume (at atmospheric pressure) bounded by inner and outer field cages and two end-plates. An electric field is created between a central membrane and the two end-plates (dividing the TPC chamber into two), giving a drift length of 2.2 *m* on each side. As charged particles pass through the chamber they leave a trail of ionized gas. The electrons drift along the electric field lines towards one of the end-plates where they induce ionization avalanches in proportional wire chambers. These are detected as pulses on cathode pads. The ϕ coordinate is calculated by interpolating the signals induced on cathode pads and the r coordinate is given by the radial position of the pads involved in the measurement. The z coordinate of a point on a track's trajectory is obtained from the electron drift time and the drift velocity.

The five helix parameters shown in Figure 2.1 are determined by fitting a helix to the pad coordinates within the first half turn of each track candidate. A

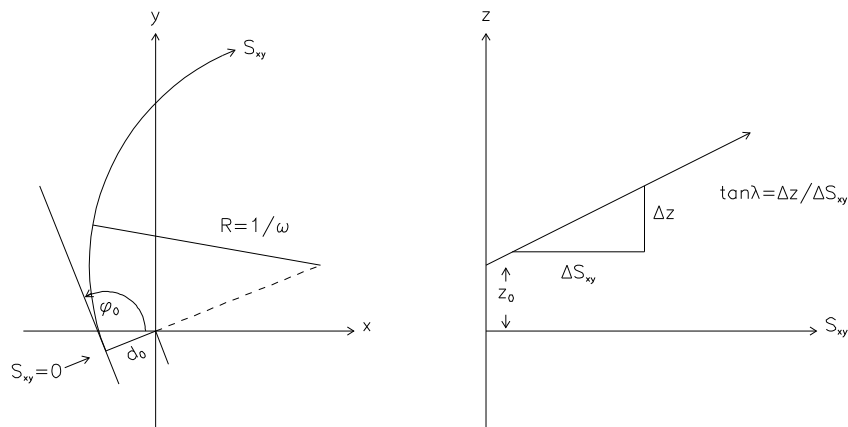


Figure 2.1: Helix parameters used in the TPC tracking algorithms. For this case all parameters are positive.

circle fit made in the xy plane yields ω (the inverse radius of curvature), d_0 (the impact parameter in the xy plane), and ϕ_0 (the emission angle in the xy plane). A straight line fit in the s_{xy} - z plane yields z_0 (the z coordinate at the closest approach to the z axis) and $\tan\lambda$ (the tangent of the dip angle). The circle fit parameters are used to calculate the values of s_{xy} .

The pulse height information on the wires provides information about the energy lost by the particle as it traverses the TPC. The rate of energy loss

(dE/dx) is dependent on the particle mass and so can be used to identify different particle species. Electron identification is good, with greater than 3σ separation up to $p \approx 8 \text{ GeV}/c$. The π - K separation is roughly constant above $p \approx 2 \text{ GeV}/c$ at about 2σ , while the K - p separation is only about 1σ . Therefore, kaon and proton identification can be accomplished only on a statistical basis; nonetheless, it is an important means of reducing combinatorial background in many analyses. The azimuthal coordinated resolution is $\sigma_{r\phi} = 180 \mu\text{m}$ at 0° pad crossing angle. The z spatial resolution for wires is $\sigma_z = 1.2 \text{ mm}$ (with a small z dependence), and 0.8 mm for pads (at $\theta = 90^\circ$).

The transverse momentum resolution and impact parameter resolution are shown in Table 2.1 for the TPC only, for the TPC and drift chamber, and for all three tracking detectors together. At low momentum (less than 0.4 GeV) a constant term of 0.5% should be added to the resolution due to multiple scattering.

2.2.3 The Principal Calorimeters

The Electromagnetic Calorimeter (ECAL)

The ECAL is a sampling proportional wire calorimeter consisting of lead sheets and proportional wire chambers covering the angular range $|\cos\theta| < 0.98$. The calorimeter stops and measures the energy of electrons and photons. The ECAL is formed from a barrel surrounding the TPC, closed at each end by an end-cap. These are divided into 12 modules, each covering an azimuthal angle of 30° . The cracks between the modules, where the ECAL is not sensitive to particles, constitute 2% of the barrel surface and 6% of the endcap surface. To ensure that the cracks in the endcaps and the barrel are not coincident the endcap modules are rotated through 15° azimuth. The modules have 45 lead/wire-chamber layers, with a total thickness of 22 radiation lengths.

Table 2.1: Momentum and impact parameter resolution for the TPC, the TPC+ITC, and the TPC+ITC+VDET. At low momentum a constant term of 0.5% should be added to the momentum resolution due to multiple scattering.

	Transverse momentum resolution (p_T in GeV)	Impact parameter resolution	
Detector	$\Delta p_T/p_T$	$\sigma_{r\phi}(\mu\text{m})$	$\sigma_{rz}(\mu\text{m})$
TPC	$1.2 \times 10^{-3} p_T$	310	808
+ ITC	$0.8 \times 10^{-3} p_T$	107	808
+ VDET	$0.6 \times 10^{-3} p_T$	23	28

The energy and position of each shower is read out using small cathode pads with dimensions $\sim (30 \times 30)$ mm arranged to form towers pointing to the interaction point; each tower is read out in three segments in depth, known as storeys, with thicknesses of 4, 9, and 9 radiation lengths respectively. There are 74,000 such towers, corresponding to an average granularity of $0.9^\circ \times 0.9^\circ$. This fine segmentation is important in the identification of photons, electrons and neutral pions. The angular resolution of the ECAL is:

$$\sigma_{\theta,\phi} = \left(\frac{2.5}{\sqrt{E}} + 0.25 \right) mrad, \quad (2.1)$$

where E is measured in GeV .

The energy resolution, determined by comparing the measured energy to the track momentum or beam energy, is shown in Figure ?? (*this is an example of a missing reference, the figure labelled FIG-ECAL-RES does not exist, the symbols ?? are shown instead of a number*) as a function of the electron energy. The corresponding fitted resolution is:

$$\frac{\sigma_E}{E} = \frac{0.18}{\sqrt{E(GeV)}} + 0.009 \quad (2.2)$$

where a linear sum is used to as it gives the best fit; using a quadratic form would give:

$$\frac{\sigma_E}{E} = \frac{0.178}{\sqrt{E(GeV)}} \oplus 0.019 \quad (2.3)$$

The energy resolution as a function of polar angle is plotted in *and so on.....*

Chapter 3

Pion Reconstruction and Initial Selection

Neutral pion candidates (or simply referred to as pions) are reconstructed from pairs of photons; candidates are either *true pions* forming a pion signal or *false pions* forming a combinatorial background. This is illustrated in Figure 3.1 where an invariant mass spectra of the photon pairs is formed.

Selecting pions from a mass window around the expected pion mass provides an initial rejection of most of the combinatorial background. A $\pm 3\sigma_M$ mass window, selecting pion candidates between a mass of $M_0 - 3\sigma_M$ and $M_0 + 3\sigma_M$, selects, in theory, 99.7% of the pion signal. M_0 is the expected mean mass of the pion candidates, normally $135 \text{ MeV}/c^2$ though there can be some energy dependence due to biases from cuts on photon energy and other detector effects. Similarly σ_M , which is given in Equation 3.1, the Gaussian width of the pion signal, also varies with pion energy:

$$\frac{\sigma_M}{M} = \frac{1}{2} \left[\frac{\sigma_{E_1}}{E_1} \oplus \frac{\sigma_{E_2}}{E_2} \oplus \frac{\sigma_{\theta_{12}}}{\tan(\theta_{12}/2)} \right] \quad (3.1)$$

where $\sigma_{\theta_{12}}$ is the spatial resolution of the calorimeter for the measured angular separation, θ_{12} , of the two photons. A correct formulation of the energy dependence of the mass window parameters is important to avoid systematic errors when estimating acceptance corrections. In this study both M_0 and σ_M are parameterized as a function of pion energy using information from reconstructed true pions. The purity of pion selection at this point depends on detector resolution, event multiplicity, the photon lower energy cut, and the momentum of the selected pions. Further improvements in selected pion purity can be gained by tightening the mass window though with a reduction in efficiency and an increase in systematic uncertainties. Momentum resolution can be improved by performing a constraint of the reconstruction pion mass to the nominal pion mass of $135 \text{ MeV}/c^2$.

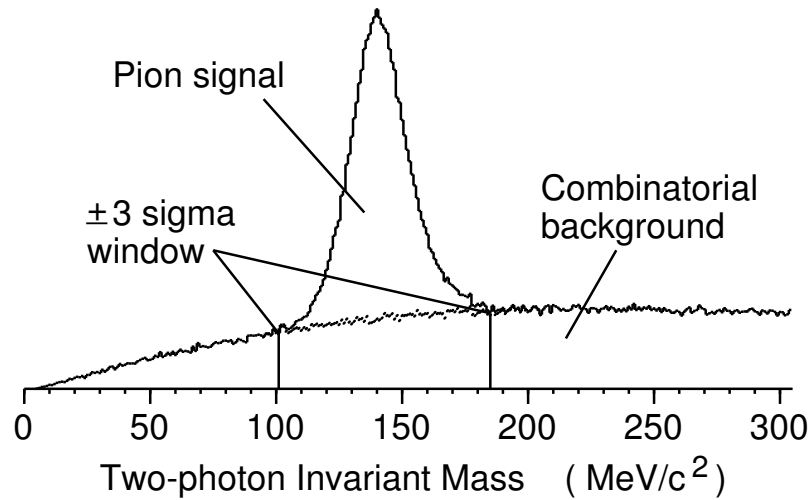


Figure 3.1: Invariant mass of photon pairs in hadronic Z decays at a center of mass energy of 91.2 GeV . The stochastic detector resolution parameter is set at $R=0.18$. All photons in this data originate from pions; correct combinations of photon pairs result in a peak representing the pion signal, incorrect combinations result in a combinatorial background forming the source of impurity in a sample of selected pion candidates. A ‘window’ around the pion peak can be selected to remove most of the background. The width of the window can be describe in terms of a number of sigmas where sigma represents the mass reconstruction resolution. A width of ± 3 sigma is common selecting almost 100% of true pions while rejecting most of the background.

3.1 Mass Constraint

The momentum resolution of π^0 is limited by the energy resolution of ECAL. One makes the assumption that the error on the opening angle θ_{12} of the photons is negligible compared to the error on their energies: in the π^0 refitting, only two photon energies are allowed to vary, while their directions are kept fixed, see [10]. The calculation is done with the well known technique of the Lagrange multipliers. If we let ω_1, ω_2 be measured energies of the two photons, and θ_{12} the opening angle between their directions, the reconstructed squared invariant mass of the π^0 is given by:

$$\mu^2 = 2\omega_1\omega_2(1 - \cos \theta_{12}) \quad (3.2)$$

We can now look at for E_1 and E_2 , the best evaluation technique of energies of the two photons, minimizing the chi-square form:

$$\chi^2 = \left(\frac{E_1 - \omega_1}{\sigma_1}\right)^2 + \left(\frac{E_2 - \omega_2}{\sigma_2}\right)^2 + \lambda(m^2 - 2E_1E_2(1 - \cos \theta_{12})) \quad (3.3)$$

where σ_1 and σ_2 are the errors on the photons energy, m is the true π^0 mass and λ is the Lagrange multiplier. We can minimize the χ^2 and get a fourth-order Equation for E_1 :

$$f(E_1) = a_4E_1^4 + a_3E_1^3 + a_1E_1 + a_0 = 0 \quad (3.4)$$

where $a_4 = \sigma_1^2/\sigma_2^2$, $a_3 = -\omega_1a_4$, $a_1 = \omega_1\omega_2^2m^2/\mu^2$ and $a_0 = \omega_1\omega_2m^2/\mu^2$.

Equation 3.4 has only two real solutions: one negative and other positive, which is only acceptable. However, since the exact solution is too complicated, we get an approximate solution linearizing Equation 3.4:

$$E_1 = \omega_1 + \left(\frac{m^2 - \mu^2}{\mu^2}\right) \frac{\omega_1\omega_2}{\sigma_1^2\omega_2^2 + \sigma_2^2\omega_1^2} \omega_2\sigma_1^2 \quad (3.5)$$

$$E_2 = \omega_2 + \left(\frac{m^2 - \mu^2}{\mu^2}\right) \frac{\omega_1\omega_2}{\sigma_1^2\omega_2^2 + \sigma_2^2\omega_1^2} \omega_1\sigma_2^2 \quad (3.6)$$

At least, one should note that the problem is further simplified when one assumes an energy resolution for photons of the form:

$$\sigma_{1,2} = R\sqrt{E_{1,2}} \quad (3.7)$$

where R is a constant, mentioned before. Putting Equation 3.7 in 3.5 and 3.6, one gets:

$$E_1 = \omega_1 + \left(\frac{m^2 - \mu^2}{\mu^2}\right) \times \frac{\omega_1\omega_2}{\omega_1 + \omega_2} \quad (3.8)$$

$$E_2 = \omega_2 + \left(\frac{m^2 - \mu^2}{\mu^2}\right) \times \frac{\omega_1\omega_2}{\omega_1 + \omega_2} \quad (3.9)$$

that is, the same quantity is added to the original photon energies.

Equation 3.8 and 3.9 are used in the **REFIT** algorithm to re-define the photon energies. Then π^0 mass is evaluated and procedure iterated until the mass is within $\pm 0.0001 \text{ MeV}/c^2$ of the nominal π^0 mass. Usually only 2 or 3 iterations are needed.

Chapter 4

A Pion Estimator

A $\pm 3\sigma_M$ mass window selection forms the starting point to study a method for improving the signal-to-background ratio. To gain further improvements in purity, cuts based on a pion estimator can be applied. The estimator is built from chi-square (χ^2) values from the mass constraint, and photon pair opening angles, θ_{12} . A plot of Chi-square versus pion opening angle, Figure 4.1, shows that true pions (circles) tend to have smaller values of chi-square and smaller opening angles than false pions (crosses). An estimator based on these two parameters can therefore be used to attempt to distinguish between correct and wrong combinations of photon pairs.

The form of the cut-off should be carefully formulated. Various functions have been investigated including rectangular and triangular shapes and ellipses; the ellipse provides the most effective function of the three alternatives, the solid curve shown in Figure 4.1, and has the form:

$$(\theta_{12}/A)^2 + (\chi^2/B)^2 = 1 \quad (4.1)$$

where the values of A and B are optimized for the data.

Optimization of the function involves a search in A and B parameter space, for this a balance between purity and efficiency must be made. A purity of 100% can be achieved by applying very tight cuts thereby rejecting all background though with only a very low selection efficiency. In most practical applications it is important, for both statistical and systematic reasons, to maintain efficiency as high as possible. The balance between efficiency and purity in this study is defined by maximizing the product of the selection efficiency and selection purity. It turns out that in general this leads to a high selection efficiency, for example for Z decays optimization using this criteria yields efficiencies between 82% and 98%.

We now consider two methods for applying the estimator with the aim of improving pion purity.

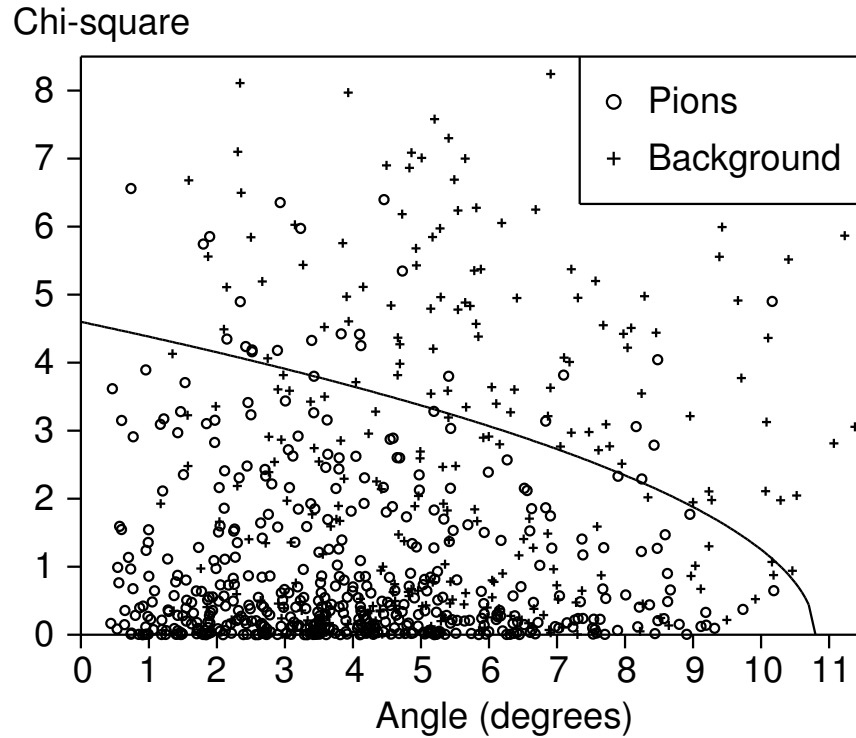


Figure 4.1: Chi-square (from a mass constraint) versus photon pair opening angle (for each pion candidate) for 300 hadronic Z decays at 91.2 GeV center of mass. True pions are represented by circles, incorrect combinations of photons yield false pions (combinatorial background) these are represented by crosses. The combinatorial background tends to have larger opening angles and chi-square values than true pions, this feature is used to discriminate between pions and background. The solid line is an ellipse of the form given in Equation 4.1 where parameters A and B have been optimized such that the product of the selection purity and efficiency is maximum. Pion candidates below the curve are selected, those above are rejected.

4.1 Estimator Application Methods

....*some sections skipped*... the purity in the Ranking method improves from 61.4% (selection efficiency of 99.5%) to 82.6% (selection efficiency of 90.6%) an improvement of 21.2%. For an event energy of 912 GeV the purity improves from 45.3% (selection efficiency of 99.3%) to 78.6% (selection efficiency of 82.0%) an improvement of 33.3%. It is interesting to note that searching through the list in reverse order or in a random order has little effect on the outcome.

The above results, together with results showing the effect of doubling detector resolution are shown in Table 4.1. More detailed comparisons of the Direct and Ranking methods are presented in the next chapter.

Table 4.1: Comparison of purity and efficiency (shown in brackets) for three pion selection methods: ‘mass window’ selection, ‘Direct estimator method’, and ‘Ranking estimator method’. The stochastic term, R , in the detector resolution, and the event energy, are varied.

Event Energy	Resolution parameter	$\pm 3\sigma_M$ mass window	Estimator cuts (Direct)	Estimator cuts (Ranking)
91.2 <i>GeV</i>	$R = 0.18$	61.4%(99.5%)	69.1% (95.1%)	82.6%(90.6%)
912. <i>GeV</i>	$R = 0.18$	45.3%(99.3%)	55.3% (92.9%)	78.6%(82.0%)
91.2 <i>GeV</i>	$R = 0.36$	46.2%(99.4%)	56.0% (92.8%)	71.9%(85.0%)

List of References

- [1] R. Barate et al. (ALEPH Collab.), *Studies of Quantum Chromodynamics with the ALEPH Detector*, Physics Reports **294** (1998) 1.
- [2] Y. Ne'eman and Y. Kirsh, Cambridge University Press, *The Particle Hunters* (1989)
- [3] Y.J. Longo, McGraw-Hill Series in Fundamentals of Physics, *Fundamentals of Elementary Particle Physics* (1973)
- [4] D.H. Perkins, *Introduction to High Energy Physics* (1987)
- [5] C. Bowdery, *ALEPH Handbook Vol.1* CERN (1995)
- [6] D. Buskulic et al. (ALEPH Collab.), *Performance of the ALEPH Detector at LEP*, Nucl. Inst. Meth. A **360** (1995) 481.
- [7] D. Decamp et al., (ALEPH Collab.), Nucl. Instr. Meth. A **294** (1990) 121.
- [8] S. Lipschuts, Schaum's Outline Series, *Probability* (1997)
- [9] G. Marchesini et al., *The Herwig Event Generator*, Comp. Phys. Comm. **67** (1992) 465.
- [10] G. Batignani et al. (ALEPH Collab.), internal note *QPI0DO: Improvement in π^0 momentum resolution using the constraint of π^0 mass.* (1993) .
- [11] M.R. Spiegel, Schaum's Outline Series, *Advanced Calculus* (1974)
- [12] N.J. Giordano, Prentice Hall, *Computational Physics* (1997)
- [13] J. Leva et al., ACM TOMS **18** (1992) 449, Fortran algorithm 454.

Appendix A

Directory Tree-Structure

Your personal directories are part of a larger directory structure of the Linux system including other users' directories and the Linux system directories. Figure A.1 illustrates, for example, the directory structure for user `ab1234`, the directories are shown relative to other user and system directories. The top

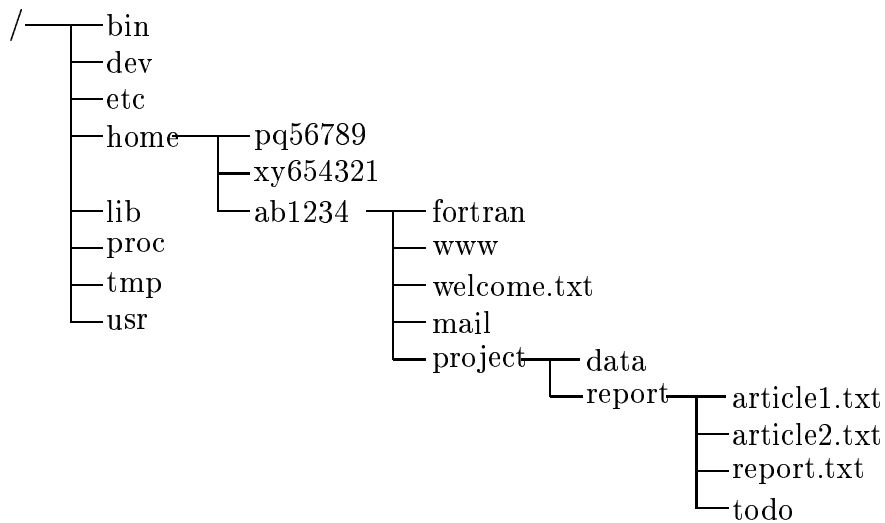


Figure A.1: A typical user's directory tree (not complete)

directory has the address `/home/ab1234/`, this can also be represented by `~/`

Publications

- [1] A. Beddall, A. Beddall, A. Bingul, Nuclear Inst. and Methods in Physics Research, A **482** (2002) 520-527.